Visualization observation of onset and damping behaviors in a traveling-wave thermoacoustic engine by infrared imaging

Bo Wang[a], Limin Qiu[a,*] , Daming Sun[a], Kai Wang[a], Weijuan Yang[b],Junhu Zhou[b]

a.Institute of Refrigeration and Cryogenics, Zhejiang University, Hangzhou 310027, PR China

b.State Key Laboratory of Clean Energy Utilization, Zhejiang University, Hangzhou 310027, PR China

Abstract

To explore the effects of Gedeon streaming on the onset and damping behaviors, infrared imaging is applied for the first time in a traveling-wave thermoacoustic engine to observe the temperature evolution of the regenerator. Under conditions of with and without Gedeon streaming, the temperature distribution differences of the regenerator in the onset and damping processes are compared and analyzed. Based on the visual images, the dimensionless temperature distribution reveals some phenomena that have not been revealed by traditional measurement methods. Analysis of the thermal and mass flows is made to further understand the mechanism of the onset and damping processes.

Key words: Thermoacoustic engine; Infrared imaging; Gedeon streaming; Regenerator; Temperature distribution.

1. Introduction

Thermoacoustic engine (TE) is a new type of long-life, non-polluting engine that can utilize thermal energy, even low grade thermal energy, with feature of no moving parts [1]. It has promising applications in the fields of electronic device cooling, natural gas liquefaction, pulse tube refrigeration, and power generation. In recent years, researchers have been making efforts to increase the output acoustic power and pressure ratio of a TE by improving the resonator [2], applying cascade or new coupling configurations[3, 4].

Onset indicates the transition of a thermoacoustic engine from the stationary to periodic oscillating state, when the temperature gradient along the regenerator is larger than the critical value (the corresponding heating temperature is so-called onset temperature). As the onset temperature determines the heat grade that a TE can utilize, the onset mechanism attracts more and more academic attentions. In fact, theoretical study including linear [5, 6], nonlinear [7], and CFD (Computational Fluid dynamics)

* Corresponding author. Tel./fax: +86 571 87952793.

E-mail address: limin.qiu@zju.edu.cn (L. Qiu).

study [8, 9] needs more detailed experimental verification. In experimental study, temperature distribution of regenerator is commonly used to analyze the onset process. Unfortunately, only discrete temperature distribution instead of temperature field can be obtained [10, 11] due to limited temperature sensors, which is insufficient for theoretical verification, especially for CFD study. Up to now, there is no visual method reported to obtain the full-scale images of the temperature distributions in TE study.

Gedeon streaming appears in the oscillating flow when there is a loop [12]. Former research shows that the Gedeon streaming significantly changes the temperature distribution of the regenerator and may seriously deteriorate the performance of a TE [1, 13-15]. In order to improve the performance of thermoacoustic engine, some methods have been proposed to suppress [1] or even eliminate (by using an elastic membrane) the Gedeon Streaming [13]. However, the onset and damping processes with the influence of Gedeon streaming have not been fullly investigated [16, 17] because of theoretical complexity and measurement difficulty.

Infrared (IR) imaging camera can conveniently obtain the visual images of the radiated heat of the objects in the absence of light. The visual temperature distribution has been successfully demonstrated as an alternative means in TE study by present authors [18]. More visual information has been obtained, which is nearly impossible with traditional methods. This inspired us to use an IR imaging camera to visually measure the temperature distribution and evolution of a thermoacoustic regenerator during the onset and damping processes.

2. Experimental apparatus

Fig. 1 illustrates the schematic of a traveling-wave TE with an IR imaging camera. The travelling-wave TE is detailed elsewhere [19], which consists of a loop and a resonator tube. The loop is composed of a heater, cooler, regenerator, feedback tube, and compliance. An elastic membrane is used to eliminate the Gedeon streaming in the TE, which is placed between the compliance and main cooler [13]. Without the membrane, the Gedeon streaming appears in the loop of the TE. The configuration when the elastic membrane used is denoted as Configurations I, and the other is Configuration II. The heating power is adjusted by changing the charging voltage to the heaters, and displayed by a digital dynamometer (QINGZHI，type ZW1603). The uncertainty of the heating power measurement is $\pm$ 11.5 W.

The pressure data acquisition system consists of pressure sensors (linear silicon piezoelectric type, KPY 46R), a data acquisition clip (NIPC-1200, 12 bit precision and a sampling frequency of 10 kHz), a computer, and a self-developed program for LabVIEW 7.1. The comprehensive error of the average pressure measurement is $\pm$ 0.0222 MPa and that of the pressure amplitude measurement is $\pm$ 6.43E-04 MPa.

The temperature data acquisition system is comprised of thermocouples, a digital

multimeter (Keithley 2700), and a digital scanner that is also displayed on the computer. Calibrated K-sheathed thermocouples are placed in the heater to measure the heating temperature, also placed near the cold and hot end of the regenerator (located on the outside wall of the regenerator, labeled as Position C and Position H, showed as C and H in Fig. 1). An IR imaging camera of FLIR SYSTEMS is used to visually measure the temperature distribution of the regenerator. The temperature range and colors of the images can be adjusted by using the software ThermaCAM QuickReport 1.1. Temperature at any position or region in an image can be obtained and exported to an Excel document.

In order to confirm the accuracy of the temperature data by IR imaging camera, temperature data in the IR images at Position C and Position H are compared (see Fig. 2) with the data by the thermocouples which are usually used in temperature measurement [20]. At Position C and H, the results by the two methods coincide well. The largest uncertainty of the temperature by thermocouples is estimated by the comprehensive error, which is ± 2.07 ℃. Fig. 2 shows that the accuracy of the temperature data by IR imaging camera is acceptable.

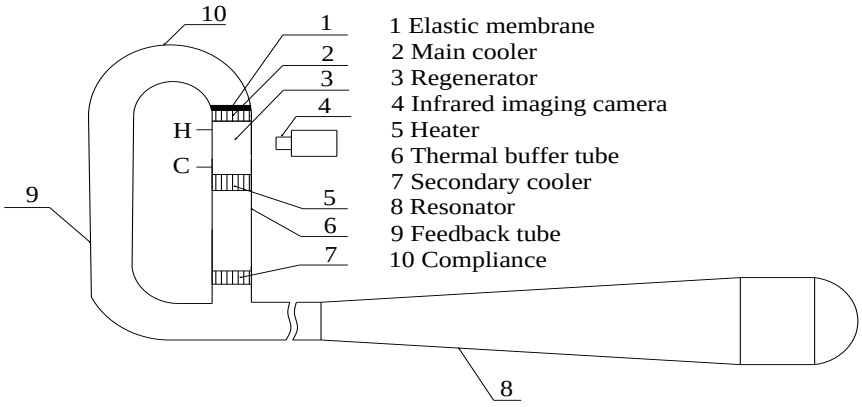


Fig. 1 Schematic of the traveling-wave TE with an infrared imaging camera

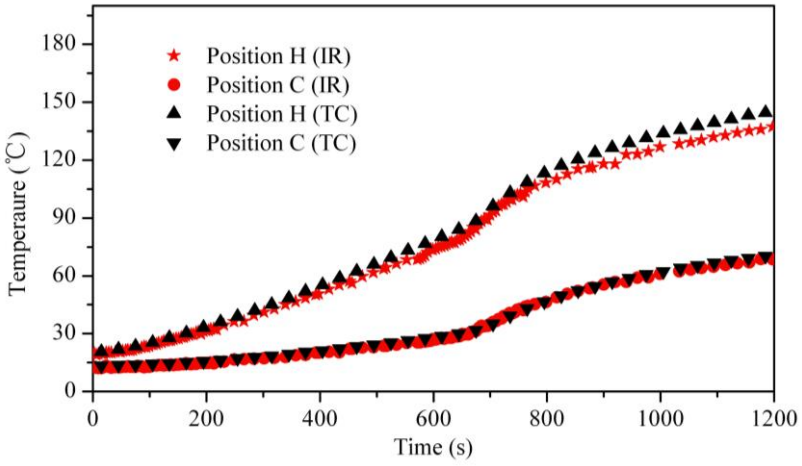


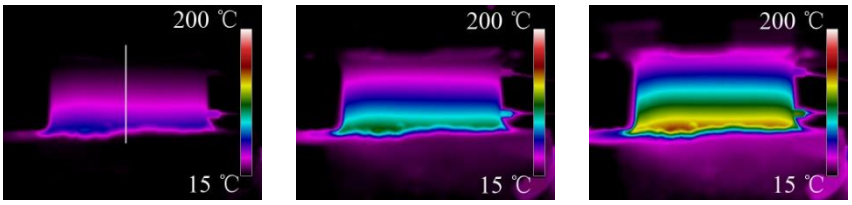
Fig. 2 Temperature measurements with the IR camera and thermocouples

3. Experimental results and analysis

3.1. Influence of Gedeon streaming on the onset process

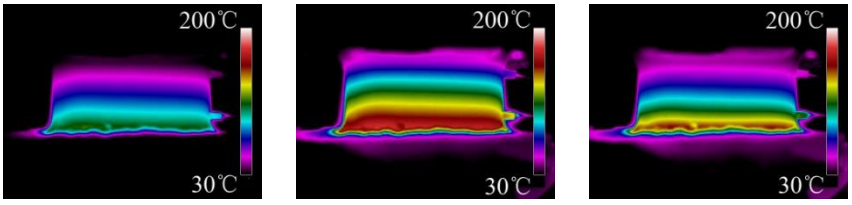
Fig. 3 shows the IR temperature distribution images of the thermoacoustic regenerator in the onset process under two conditions: without and with Gedeon streaming. The temperature of all the images is adjusted in the range of 15-200 ℃ without streaming, and 30-200 ℃ with streaming. The black region represents the lowest temperature, while the white is the highest. All the images display obvious color separation in the axial direction of the regenerator, indicating the existence of temperature gradient along the regenerator. The same color which indicates the same temperature is ideally horizontal in the central part of the images. Note that the radiation angle is responsible for the lower curve at the edge of the images, as the IR camera receives less thermal radiation from the edge of the regenerator.

The heating power is maintained at 1000 W under both conditions. Before onset, the phenomena in Fig. 3-I and 3-II are similar: the regenerator temperature gradually increases and temperature gradient rises. When the gradient is larger than the critical value, onset occurs (B in Fig. 3). After onset, the phenomena are different: without streaming the regenerator temperature continues to increase, while with streaming the regenerator temperature decreases after onset.



A .298 s before onset, about 5 min, T_H=86℃ | B. onset, T_H=157℃ | C. 180 s after onset, 3 min, T_H=182℃

I. **without** streaming



A. 372 s before onset, about 6 min, T_H=142℃ | B. onset, T_H=216℃ | C. 108 s after onset, about 2 min, T_H=225℃

II. **with** streaming

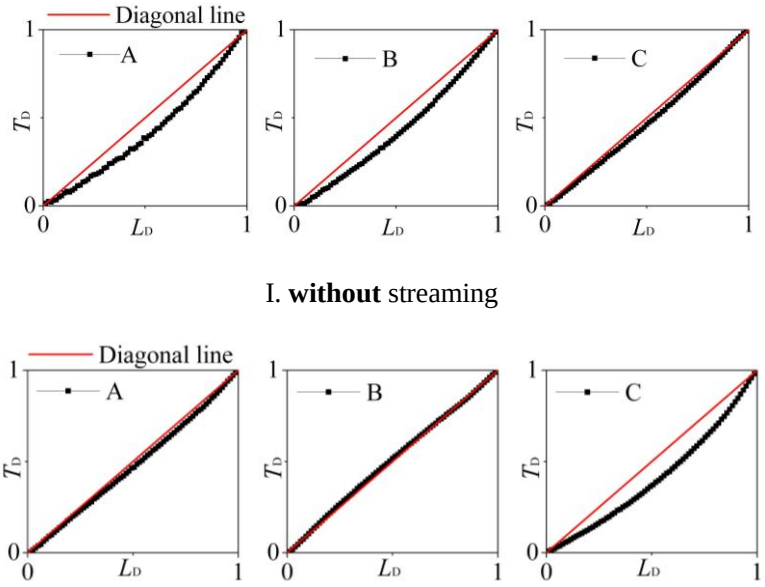
Fig. 3 IR images of the regenerator in the onset process

The temperature distributions of the regenerator along the axial direction are collected (see Fig. 3-I.A, shown as the white line) and displayed in Fig. 4, with the non-dimensional length L_D as the horizontal axis and non-dimensional temperature T_D

as the longitudinal axis. The definition $L_D = L/\Delta L$, where L is the distance away from the cold end of the regenerator and ΔL is the total length of the regenerator; $T_D = (T - T_C)/(T_H - T_C)$, where T, T_H, and T_C represent the regenerator temperature at the position of L, hot end and cold end. Without Gedeon streaming the temperature distribution of the regenerator is nonlinear before onset (Figs. 4-I.A, the moments of A, B, C in Fig. 4 correspond with that in Fig. 3), which evolves to be linear after onset (Fig. 4-I.C). With streaming the distribution is different, which is linear before onset and nonlinear after onset.

The reasons can be analyzed from Fig. 5. Without Gedeon streaming before onset, the small heat conduction in the axial direction between the stainless steel (SS) meshes in the regenerator (labeled as Q_{cond}) and large heat leakage in the radial direction (labeled as Q_{leak}. In this direction conduction of the SS meshes is good enough, in addition, the outside wall of the regenerator is not insulated) make the regenerator temperature lower than the linear temperature, so the temperature distribution line lies below the diagonal line. There is also the upward natural convection $Q_{natural}$ generated in the heater, regenerator, and main cooler of the TE, which causes a higher distribution line than the linear. The elastic membrane nearly gets rid of $Q_{natural}$, so the small Q_{cond} and large Q_{leak} are dominantly responsible for the temperature distribution line and makes it lower than the linear. In a traveling-wave TE the penetration depth of the gas is much larger than the characteristic dimension of the SS meshes, sufficient heat transfer between the gas and meshes makes the temperature distribution change to be linear as soon as onset occurs (see Fig. 4-I.C). Many repeated experiments conducted under the same condition shows the same results. So the above-mentioned figures, especially the temperature distribution difference before and after onset in Fig. 4, are credible. In our previous experiments in Configuration I, using the limited number of thermocouples, the distribution difference can not be observed before and after onset [14].

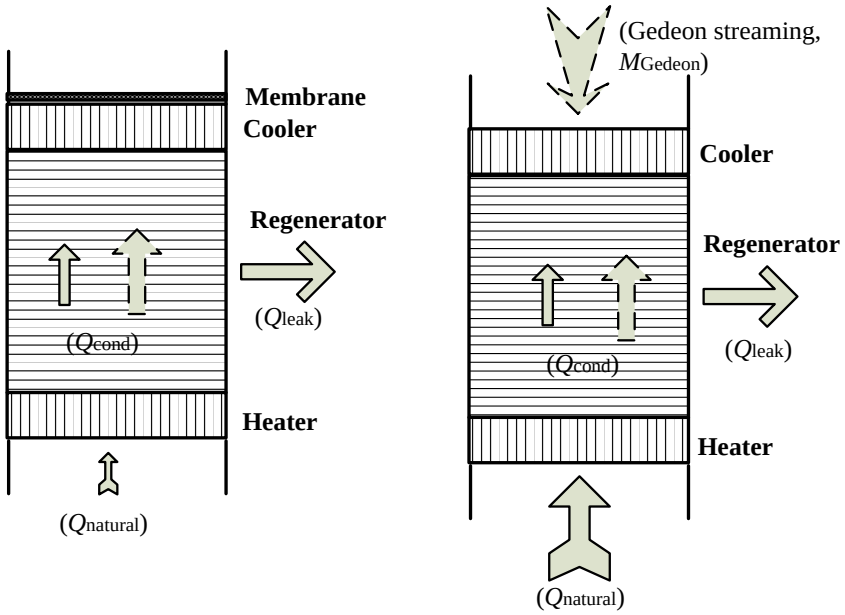
In Configuration II, before onset the small Q_{cond} and large Q_{leak} make the distribution line lower than the diagonal line. The intense natural convection $Q_{natural}$ makes the distribution line above the diagonal line, as the convective gas can go up easily from the heater to the regenerator without the elastic membrane. They have close effect on the distribution line, so it turns out to be linear before onset (Fig. 4-II.A) and at the onset point (Fig. 4- II.B). After onset, the Gedeon streaming (M_{Gedeon}) makes the temperature distribution change and lie blow the diagonal line. Judged from Fig. 4- II.C, the direction of the streaming is from the main cooler to the regenerator and to the heater. In our previous experiments in Configuration II, using the limited number of thermocouples, the nonlinear temperature distribution after onset can also be observed. But it can not characterize the clear distribution before onset [14].



I. **without** streaming

II. **with** streaming

Fig. 4 Axial temperature distribution in the regenerator in onset process. The diagonal line implies a linear temperature distribution in the regenerator.



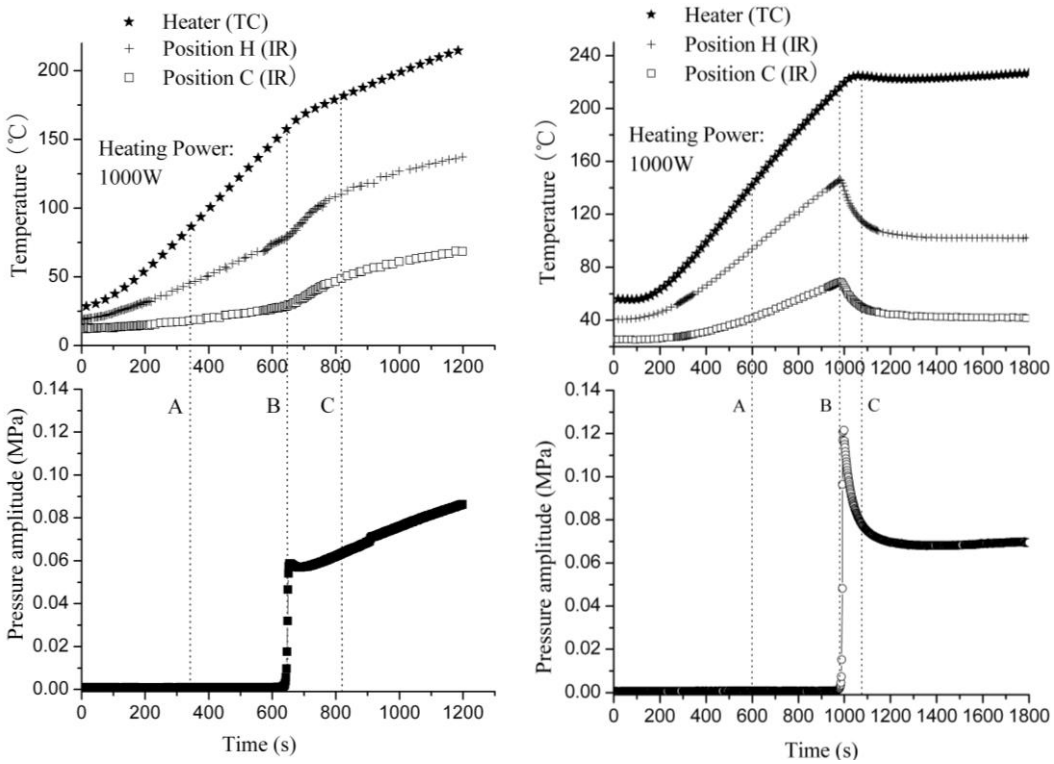
I. **without** streaming II. **with** streaming

Fig. 5 Thermal and mass flows in the regenerator in the onset process. The solid arrows of thermal conduction Q_{cond} along SS meshes represent that before onset and the dotted ones of Q_{cond} and M_{Gedeon} represent that after onset.

Fig. 6 shows the dependence of pressure and temperature collected simultaneously. 0 s represents the instant when the heater starts heating the TE. The moments of A, B, C in Fig. 6 also correspond with that in Figs. 3 and 4. The temperature and pressure evolution during the onset process shows the differences between the two conditions

without and with the streaming. Without Gedeon streaming before onset (I.A-I.E) the heater and regenerator temperature gradually increases, reaching the critical value when onsets (I.F). Under the condition with streaming, before onset the temperature evolution is similar with that without streaming. Obvious difference appears after onset, that the regenerator temperature decreases sharply, which is caused by the Gedeon Streaming in the loop that leads to a change of the temperature distribution.

The pressure amplitude experiences a sudden increase at onset moment under both conditions (see Fig. 6). Without streaming, the amplitude increase to 0.06 MPa and with streaming it increases to 0.12 MPa. After onset, without streaming, the pressure amplitude continues increasing, while with streaming it decreases sharply because the Gedeon streaming deteriorates the performance of the TE. The pressure amplitude at onset moment with streaming is much larger (about 2 times) than that without streaming.



I. **without** streaming II. **with** streaming

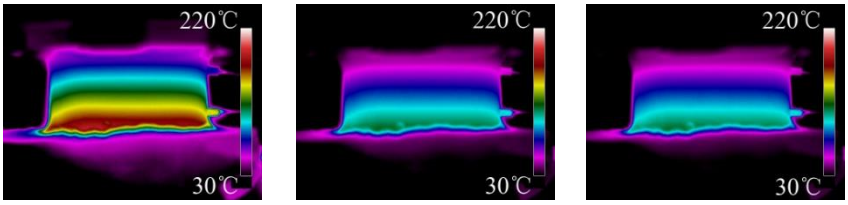
Fig. 6 Pressure and temperature evolution in the onset process

3.2. Influence of Gedeon streaming on the damping process

As the opposite process of onset, damping indicates the moment when the oscillating flow stops, which can enhance the understanding of the onset process and performance of the regenerator.

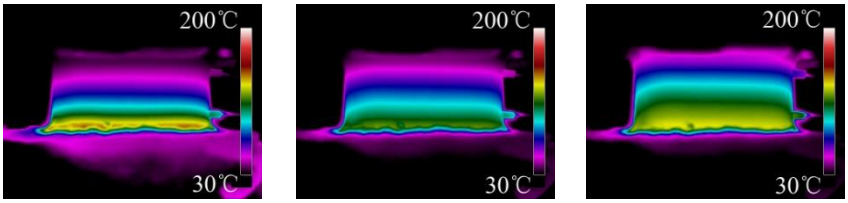
Fig. 7 shows the IR images during the damping process without and with the Gedeon streaming. After the heating power stops, the damping process begins and the

regenerator temperature decreases under both conditions. The pressure amplitude also decreases until the thermoacoustic oscillation disappears (see Fig. 8), the time when the pressure amplitude being zero is named as disappearing moment. Difference appears after disappearing moment (which can be seen from Figs. 7 and 8). Without streaming, the regenerator temperature keeps on decreasing while with streaming the temperature rises. The reason is that after disappearing moment, Gedeon streaming disappears and the natural convection becomes the dominant factor influencing the temperature distribution, which leads to the rebuilding of the temperature distribution.



a. damping begins, T_H=234℃ | b. **disappearing moment,** T_H=162℃ | c. 38 s after disappearing, T_H=161℃

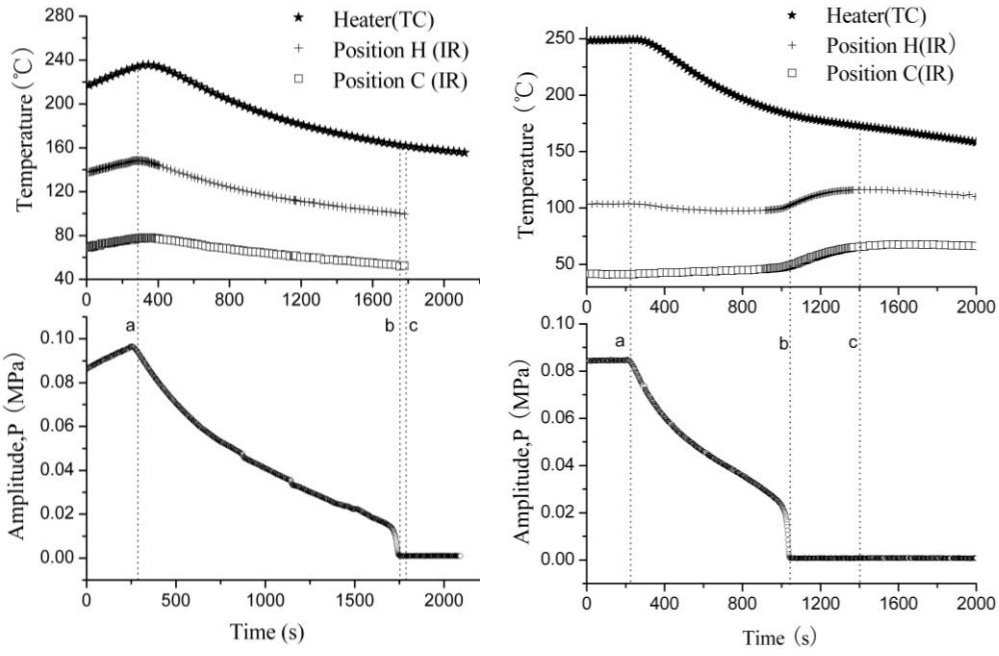
I. **without** streaming



a. 820 s before disappearing, T_H=249℃ | b. **disappearing moment**, T_H=182℃ | c. 360 s after disappearing , T_H=173℃

II. **with** streaming

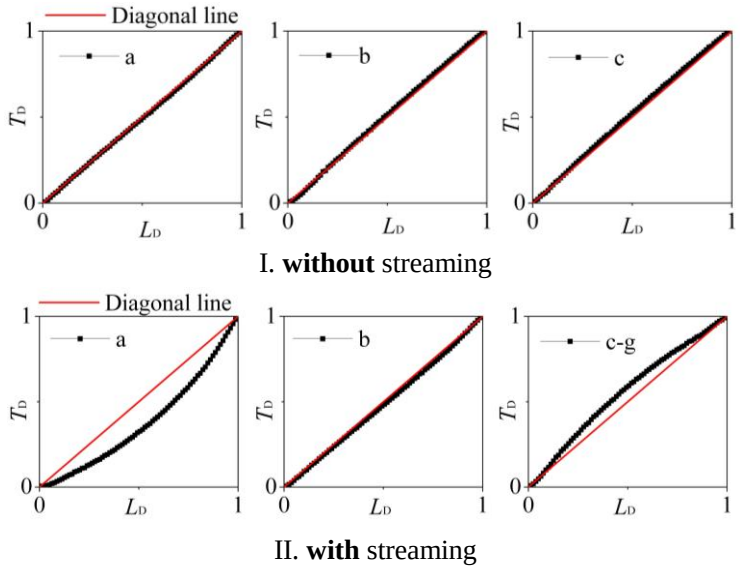
Fig. 7 IR images in damping process, where disappearing means the thermoacoustic oscillation disappears.



I. **without** streaming II. **with** streaming

Fig. 8 Pressure and temperature evolution in damping process

The temperature distributions are analyzed in Fig. 9. Fig. 5 can also be used to discuss the reasons, where the solid and dotted arrows have different meanings. The dotted arrows of Q_{cond} and M_{Gedeon} represent the thermal and mass flows before disappearing moment, the solid ones of the Q_{cond} represent that after disappearing moment. Without Gedeon streaming before disappearing moment, the temperature distributions are linear in Fig. 9-I.a. Q_{leak} makes the distribution line lower than the diagonal line and $Q_{natural}$ makes it higher than the linear, the sufficient heat transfer Q_{cond} dominates the distribution and makes the distribution linear. After disappearing moment, Q_{cond} becomes much smaller as the oscillating flow stops, $Q_{natural}$ dominates the distribution and makes it a little higher than the diagonal line. With Gedeon streaming, the temperature distributions are much more complicated. Before disappearing moment in Fig. 9-II.a, there are large heat transfer Q_{cond}, large Q_{leak}, upward $Q_{natural}$, and downward Gedeon streaming M_{Gedeon} which dominates the distribution, thus the distribution line lies lower than the diagonal line. In Fig. 9-II.b near the disappearing moment the Gedeon streaming disappears, Q_{cond} becomes much smaller, Q_{leak} and $Q_{natural}$ come to a balance and make the distribution linear. After disappearing moment in Fig. 9-II.c, the upward $Q_{natural}$ dominates the distribution and makes it higher than the linear line.



I. **without** streaming

II. **with** streaming

Fig. 9 The axial temperature distribution in the regenerator in the damping process

Fig. 8 also gives the pressure amplitude change during the damping process. The amplitude decreases to 0 MPa within a short time under both conditions. It is difficult for the TE to maintain oscillating because of the Gedeon streaming, thus with streaming, the TE damps at much higher pressure amplitude, compared with the condition without streaming.

To summarize, for the experimental cases discussed in this paper, during the onset and damping processes, the regenerator temperature distribution depends on below

factors: thermal conduction between the SS meshes in the axial direction of the regenerator Q_{cond}, heat leakage in the radial direction Q_{leak}, upward natural convection $Q_{natural}$, and Gedeon streaming M_{Gedeon}.

4. Discussion

IR imaging is an indirect measurement method for characterizing the regenerator temperature distribution. It measures the regenerator wall which is not insulated. The traditional method using thermocouples also measures the outside wall of regenerator, which is covered by asbestos. They are used to estimate the internal distribution of regenerator based on the hypothesis: 1) the thickness of the tube wall is small enough that the heat conduction along the tube wall from the heater to the cooler can be neglected. 2) The stainless steel meshes are stacked layer by layer inside the regenerator, thus the heat conduction in the radial direction is much better than that in the axial direction. These two reasons make it reasonable to relate the outside temperature distribution to the inside one.

However, the outside distribution can not absolutely reflect the internal distribution. The CFD (2d) calculation results of the temperature distributions only considering the heat conduction inside the regenerator show the influence of insulation conditions (see Fig.10).

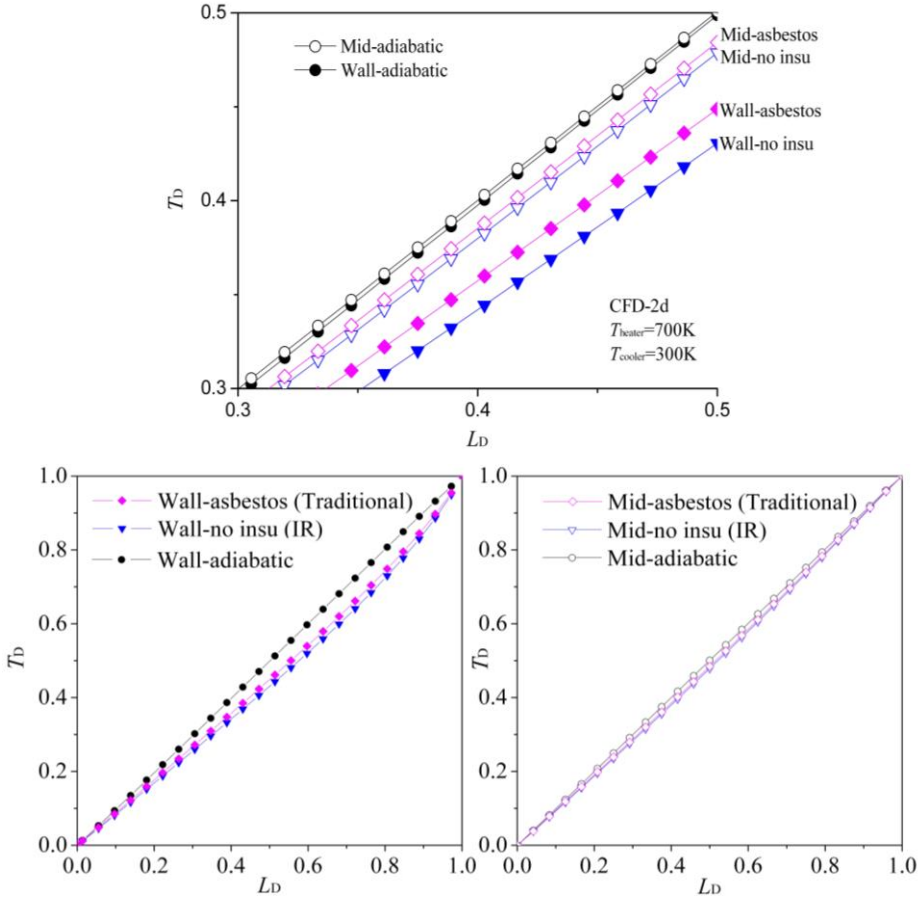


Fig. 10 Influence of insulation conditions on the temperature distribution. The flow and heat transfer of gas inside the regenerator is not considered.

Insulation condition has relatively small impact on the temperature distribution in the middle of the regenerator. Close distribution appears under the conditions of adiabatic (absolutely insulated, impossible in experiments), asbestos insulation (2 cm thick), and without insulation (the outside wall is open to air). The distribution is almost linear under adiabatic condition. Under the other two conditions, the distribution line is a little lower than the diagonal line, which is caused by the small heat conduction in the axial direction Q_{cond} and large heat leakage $Q_{leak.}$

Insulation condition has relatively large impact on the temperature distribution of the outside wall of the regenerator. The wall temperature distribution is almost linear under adiabatic condition. Under conditions with asbestos and without insulation the distribution is very close with the distribution line lower than the diagonal line. There is deviation from the distribution in the middle of regenerator. However, the tendency outside and inside the regenerator is the same and the deviation is small.

IR imaging and thermocouples can obtain the close temperature distribution of the wall. In experiments, thermocouples are used with number limitation (In our previous experimental study, only 3 thermocouples were located along the axial direction of the regenerator, and the number is not sufficient), and the IR imaging represents its advantages and can represents clear temperature distribution.

5. Conclusion

Using an IR imaging camera as a means of characterizing temperature distributions of thermoacoustic regenerators, the visual IR images have been obtained for the first time in TE study. The visual IR images enhanced the understanding of the dynamic processes of onset and damping without and with Gedeon streaming in the loop of the TE. When the outside wall of the regenerator is not insulated, without Gedeon streaming, the axial temperature distribution is nonlinear before onset and linear after onset. With Gedeon streaming, the distribution is linear before onset, in the damping process, the nonlinear distribution converts to linear, then to nonlinear. As the basis of simulation, IR visual images can supply abundant information of temperature field to support the theoretical study, such as CFD study.

Acknowledgement

The project is supported by National Funds for Distinguished Young Scientists of China under contract No. 50825601 and the program for new century excellent talents in university under contract No. NCET-06-0521

References

[1] S. Backhaus, G.W. Swift, A thermoacoustic-Stirling heat engine: Detailed study, J. Acoust. Soc. Am., 107(6) (2000) 3148-3166.

[2] E.C. Luo, H. Ling, W. Dai, Y. Zhnag, A high pressure-ratio, energy-focused thermoacoustic heat

engine with a tapered resonator, Chin. Sci. Bull., 50(3) (2005) 284-286.

[3] D.L. Gardner, G.W. Swift, A cascade thermoacoustic engine, J. Acoust. Soc. Am., 114(4) (2003) 1905-1919.

[4] W. Dai, E.C. Luo, J.Y. Hu, Y.Y. Chen, A novel coupling configuration for thermoacoustically-driven pulse tube coolers: Acoustic amplifier, Chin. Sci. Bull., 50(18) (2005) 2112-2114.

[5] M. Watanabe, A. Prosperetti, H. Yuan, A simplified model for linear and nonlinear processes in thermoacoustic prime movers .1. Model and linear theory, J. Acoust. Soc. Am., 102(6) (1997) 3484-3496.

[6] A.T.A.M. de Waele, Basic treatment of onset conditions and transient effects in thermoacoustic Stirling engines, J. Sound. Vib., 325(4-5) (2009) 974-988.

[7] H. Yuan, S. Karpov, A. Prosperetti, A simplified model for linear and nonlinear processes in thermoacoustic prime movers. Part II. Nonlinear oscillations, J. Acoust. Soc. Am., 102(6) (1997) 3497-3506.

[8] J.A.L.A. Nijeholt, M.E.H. Tijani, S. Spoelstra, Simulation of a traveling-wave thermoacoustic engine using computational fluid dynamics, J. Acoust. Soc. Am., 118(4) (2005) 2265-2270.

[9] G.Y. Yu, E.C. Luo, W. Dai, J.Y. Hu, Study of nonlinear processes of a large experimental thermoacoustic-Stirling heat engine by using computational fluid dynamics, J. Appl. Phys., 102(7) (2007) 074901-074901~074901-074907.

[10] K.I. Matveev, G.W. Swift, S. Backhaus, Analytical solution for temperature profiles at the ends of thermal buffer tubes, Int. J. Heat Mass Transfer, 50(5-6) (2007) 897-901.

[11] L.M. Qiu, D.M. Sun, Y.X. Tan, W.L. Yan, P. Chen, L. Zhao, G.B. Chen, Effect of pressure disturbance on onset processes in thermoacoustic engine, Energ. Conv. Manage., 47(11-12) (2006) 1383-1390.

[12] D. Gedeon, DC gas flows in Stirling and pulse-tube cryocoolers., Plenum, New York, 1997.

[13] L.M. Qiu, D.M. Sun, Y.X. Tan, X. Deng, G.B. Chen, Investigation on Gedeon streaming in a traveling wave thermoacoustic engine, in: J.G. Weisend, J. Barclay, S. Breon, et, al. (Eds.) Proceedings of Cryogenic Engineering Conference, Advances in Cryogenic Engineering, Keystone, CO, 2005, pp. 1115-1122.

[14] Y.X. Tan, L.M. Qiu, D.M. Sun, J.P. Zheng, Investigation on streaming in a Stirling thermoacoustic engine, Cryogenic Enginnering, 151(3) (2006) 16-32 (in Chinese).

[15] G.W. Swift, D.L. Gardner, S. Backhaus, Acoustic recovery of lost power in pulse tube refrigerators, J. Acoust. Soc. Am., 105(2) (1999) 711-724.

[16] G. Penelet, E. Gaviot, V. Gusev, P. Lotton, M. Bruneau, Experimental investigation of transient nonlinear phenomena in an annular thermoacoustic prime-mover: observation of a double-threshold effect, Cryogenics, 42(9) (2002) 527-532.

[17] G. Penelet, V. Gusev, P. Lotton, M. Bruneau, Nontrivial influence of acoustic streaming on the efficiency of annular thermoacoustic prime movers, Phys. Lett. A, 351(4-5) (2006) 268-273.

[18] B. Wang, L.M. Qiu, D.M. Sun, Y. Liu, Y. Yu, Infrared imaging as a means of characterizing temperature distributions of thermoacoustic regenerators, in: Proceedings of Heat Powered Cycles, TU Berlin, 2009.

[19] D.M. Sun, L.M. Qiu, W. Zhang, W.L. Yan, G.B. Chen, Investigation on traveling wave thermoacoustic heat engine with high pressure amplitude, Energ. Conv. Manage., 46(2) (2005) 281-291.
[20] K.I. Matveev, G.W. Swift, S. Backhaus, Temperatures near the interface between an ideal heat exchanger and a thermal buffer tube or pulse tube, Int. J. Heat Mass Transfer, 49(5-6) (2006) 868-878.